Journal of Theoretical Biology 398 (2016) 20–31

Contents lists available at ScienceDirect

Journal of Theoretical Biology

journal homepage: www.elsevier.com/locate/yjtbi

Turgidity-dependent petiole flexibility enables efficient water use by a tree subjected to water stress

David Gonzalez-Rodriguez [a,*,1], Paul-Henry Cournède [b], Emmanuel de Langre [a]

[a] Hydrodynamics Laboratory (LadHyX), École Polytechnique, 91128 Palaiseau, France
[b] MAS Laboratory, École Centrale Paris, 92160 Châtenay-Malabry, France

HIGHLIGHTS

- A multiphysics model of the role of wilting in the tree response to water stress is proposed.
- The model couples petiole mechanics, thermal energy balance, and xylem hydraulics.
- Turgidity-dependent petiole flexibility can significantly reduce the risk of cavitation.
- Petiole flexibility increases water use efficiency under water stress.

ARTICLE INFO

Article history:
Received 27 August 2015
Received in revised form
25 February 2016
Accepted 5 March 2016
Available online 15 March 2016

Keywords:
Water stress
Drought
Wilting
Leaf
Turgor pressure
Cavitation
Photosynthesis
Biomechanics

ABSTRACT

Water stress is a major cause of tree mortality. In response to drought, leaves wilt due to an increase in petiole flexibility. We present an analytical model coupling petiole mechanics, thermal balance, and xylem hydraulics to investigate the role of petiole flexibility in protecting a tree from water stress. Our model suggests that turgidity-dependent petiole flexibility can significantly attenuate the minimal xylem pressure and thus reduce the risk of cavitation. Moreover, we show that petiole flexibility increases water use efficiency by trees under water stress.

1. Introduction

Drought is a major cause of tree mortality, whose incidence is rising due to climate change (Allen et al., 2010). While the processes by which drought kills trees remain an issue of ongoing debate and study, McDowell et al. (2008) advanced two dominant mechanisms of drought-induced tree mortality: carbon starvation and hydraulic failure. Carbon starvation arises from the reduction of photosynthetic carbon assimilation during water stress. If drought lasts for a sufficiently long time, the carbon reserves stored by the tree will be exhausted and metabolism will be impaired. Carbon starvation thus inhibits tree growth and renders the tree more susceptible to insect attacks and to pathogens (McDowell et al., 2008). Hydraulic failure involves xylem cavitation, which can significantly reduce the tree's hydraulic conductivity and impair sap flow. Hydraulic failure usually occurs during a particularly severe drought episode that generates very negative hydraulic pressures in the xylem.

As conceptualized by several authors (McDowell et al., 2008; Sade et al., 2012), isohydric and anisohydric trees exhibit two different strategies in response to water stress. Isohydric trees attenuate variations of their leaf water potential, notably by regulating stomatal aperture, thus reducing transpiration and protecting themselves from cavitation. However, stomatal closure in isohydric trees also reduces photosynthetic carbon assimilation, thus increasing their vulnerability to carbon starvation. In contrast, anisohydric trees regulate stomatal conductance and leaf water

* Corresponding author.
E-mail address: davidgr@alum.mit.edu (D. Gonzalez-Rodriguez).
[1] Present address: Laboratory LCP-A2MC, Université de Lorraine - Metz, 57070 Metz, France.

http://dx.doi.org/10.1016/j.jtbi.2016.03.011
0022-5193/

potential less markedly, potentially making them more prone to cavitation.

Under water stress, tree leaves experience wilting. Indeed, wilting is a visual indicator of water stress and of the likelihood of tree survival (Engelbrecht et al., 2007). Leaf wilting is caused by the reduction of turgor pressure, which induces a decrease of the petiole's elastic modulus (Nilsson et al., 1958). Several experimental studies have suggested that leaf wilting may protect against water stress. In an experiment with tropical forest trees whose leafs were either mechanically constrained to remain at their turgid orientation or let free to wilt, Chiariello et al. (1987) showed that leaf wilting increases water use efficiency (the ratio of carbon assimilation to water loss by transpiration) by 15–60%. Moreover, Zhang et al. (2010) showed that leaf wilting, while decreasing photosynthesis in the short term, protects leaves from damage by excessive light irradiation, thus preserving higher photosynthetic rates in the long term.

In this paper we investigate the role of petiole flexibility in protecting a tree from water stress. It is emphasized that by the shortcut *petiole flexibility* we refer to the mechanism by which the petiole's elastic modulus decreases with decreasing turgor pressure, thus inducing leaf wilting. Whereas the conceptual framework we present is extensible to a variety of plants, in this paper we specifically focus on trees, since we account only for turgidity-dependent flexibility of leaf petioles, but not of stems or laminae. In the following we present an analytical model coupling petiole mechanics, heat exchange in the leaf, and tree hydraulics. We study two paradigms of stomatal response to water stress, corresponding to isohydric and anisohydric behaviors. Our model allows us to investigate how petiole flexibility modulates xylem pressure and photosynthetic assimilation in a tree subjected to water stress.

2. Model

We consider an idealized tree whose leaves are located at the top of a single vertical trunk of height h. As represented in Fig. 1, we consider two model geometries: a uniform foliage (Fig. 1A), where all N leaves have identical inclination, or a distributed foliage (Fig. 1B), where we define a probability distribution of the branch and leaf inclination angles, as discussed in Section 2.6. The leaves are connected to the trunk by flexible petioles, whose elastic modulus depends on the turgor pressure. We model the following coupled physical phenomena: (1) thermal energy balance in the leaves, which determines the leaf temperature, $T_l^{(i)}$; (2) transpiration from leaves, which determines the total transpiration flow rate, Q_T; (3) the hydrodynamics of sap ascent in the xylem, which determines the turgor pressure in the petioles, p_t; and (4) the solid mechanics of a petiole, which determines the leaf's angle of inclination with respect to the vertical direction, $\phi^{(i)}$. The superindex (i), used in some of the model variables, refers to leaf $i \in \{1, 2, ...N\}$. It denotes variables that, in the distributed foliage model, take different values for different leaves. For a list of parameters and variables used in the model, the reader is referred to Tables 1 and 2.

In each of the following subsections, we start from rather general equations describing each of the four key physical processes involved. We introduce a number of assumptions that allow us to simplify the governing equations. In Section 3, we will apply the simplified equations to study the tree response to water stress for several cases: uniform or distributed foliage, constant or variable stomatal opening, and rigid or flexible petioles.

2.1. Thermal energy balance in the leaf

The leaf energy balance equation is (e.g., Nobel, 2005; Leigh et al., 2012):

$$t_l C_l \frac{dT_l^{(i)}}{dt} = Q_{rad} - \alpha(T_l^{(i)} - T_a) - \frac{L\rho q_{T,l}^{(i)}}{A_l}. \quad (1)$$

This equation states that the change in thermal energy in the leaf equals the balance between the radiative energy flux (first term on the right-hand side, Q_{rad}), the convective energy flux (second term), and the evaporative energy flux (third term). Here t_l is the leaf thickness, C_l is the thermal capacity of the leaf (J m^3 K^{-1}), T_a and $T_l^{(i)}$ are respectively the air and leaf temperatures, L is the latent heat for evaporation of water (J kg^{-1}), ρ is the water density, $q_{T,l}^{(i)}$ is the flow rate of transpiration through leaf i (m^3 s^{-1}), and A_l is the leaf surface area. The heat transfer coefficient is given by $\alpha = Nu\, k/d$, where $k = 0.026$ W m^{-1} K^{-1} is the thermal conductivity of air, d is the diameter of the leaf (defined as the diameter of the largest circle that can be inscribed within the leaf surface), and Nu is the Nusselt number, which represents the heat

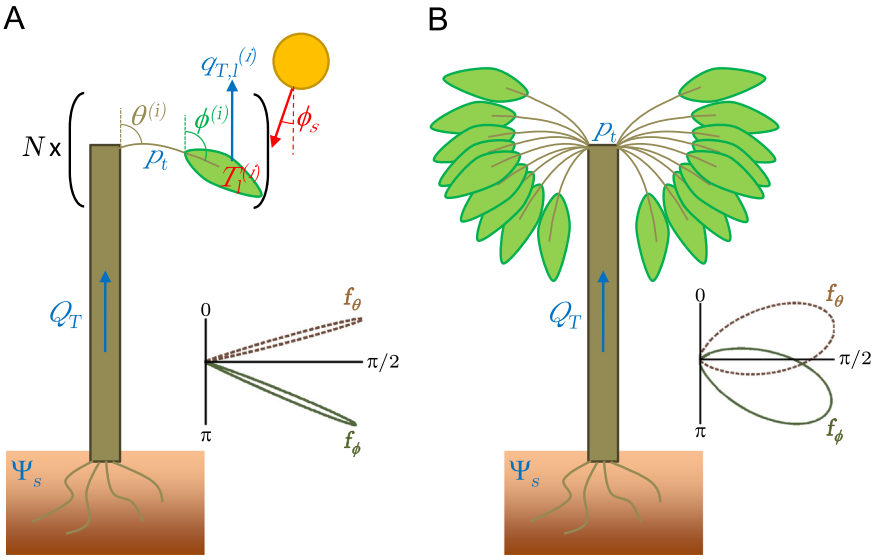

Fig. 1. (A) Sketch of the uniform foliage model showing the parameters defining the branch, leaf, and sun inclination angles. (B) Sketch of the distributed foliage model. The insets show polar plots of the corresponding BIADs (branch inclination angle distributions, brown dashed lines) and LIADs (leaf inclination angle distributions, green solid lines), as in Tadrist et al. (2014). (For interpretation of the references to color in this figure caption, the reader is referred to the web version of this paper.)

Table 1
Typical values of the dimensional parameters for a tree, obtained from Nobel (2005) and Leigh et al. (2012).

Parameter	Symbol	Reference value	Variability range
Leaf visible light absorptance	a_V	0.6	0.4–0.6
Leaf infrared absorptance	a_{IR}	0.96	0.94–0.98
Leaf infrared emissivity	e_{IR}	0.96	0.94–0.98
Reflectance of the surroundings	r	0.2	0.10–0.30
Direct zenithal solar radiation	S_0	900 W m^{-2}	500–1100
Stefan–Boltzmann constant	σ	5.67×10^{-8} W m^{-2} K^{-1}	N/A
Effective temperature of the sky	T_{sky}	250 K	220–270
Effective temperature of surroundings	T_{surr}	300 K	290–315
Air temperature	T_a	300 K	290–315
Relative air humidity	H	0.50	0.30–0.70
Wind speed	u_{wind}	1 m s^{-1}	0.3–10
Leaf inscribed diameter	d	0.10 m	0.05–0.30
Leaf surface area	A_l	10^{-2} m^2	2.5×10^{-3}– 0.09
Number of leaves	N	10^5	5×10^4–10^6
Tree height	h	20 m	10–30
Latent heat of evaporation	L	2.26×10^6 J kg^{-1}	N/A
Molar volume of water	V_{mw}	18×10^{-6} m^3 (mol H_20)$^{-1}$	N/A
Maximum stomatal conductance	g_1	0.1 (mol vapor) m^{-2} s^{-1}	0.01–0.5
Total flow resistance	R_X	10^{10} Pa s m^{-3}	10^9–10^{11}
Turgor pressure at $E_G=1$	$p_t^{(0)}$	2×10^5 Pa	10^5–4×10^5
Petiole's osmotic pressure	Π	1.1×10^6 Pa	10^5–2×10^6
Soil water potential	Ψ_s	-3×10^5 Pa	-2×10^6

Table 2
Variables used in the model.

Symbol	Meaning	SI units
g_s	Stomatal conductance	(mol vapor) m^{-2} s^{-1}
$\hat{g}$	Nondimensional stomatal conductance	
p_t	Turgor pressure in the petioles	Pa
$\hat{p}_t$	Nondimensional turgor pressure in the petioles	
Q_T	Total transpiration flow rate	m^3/s
$q_{T,l}^{(i)}$	Transpiration flow rate through leaf i	m^3/s
$\hat{q}_{T,l}^{(i)}$	Nondimensional transpiration flow rate through leaf i	
$T_l^{(i)}$	Temperature of leaf i	K
$\Delta\hat{T}^{(i)}$	Nondimensional leaf-to-air temperature difference for leaf i	
$w_l^{(i)}$	Humidity at leaf i	mol H_2O/mol air
$\Delta\hat{w}^{(i)}$	Nondimensional leaf-to-air humidity difference for leaf i	
$\theta^{(i)}$	Branch inclination angle for leaf i	rad
$\phi^{(i)}$	Inclination angle of leaf i	rad

transfer increase due to flow convection. Determination of Nu depends on whether heat convection is forced (governed by the wind) or free (governed by air buoyancy). Wind-dominated heat convection requires a Reynolds number larger than about 3000, which is almost ubiquitously attained in trees (for a $d=10$ cm leaf, $Re=3000$ already for the very low wind speed of 0.5 m/s). For this reason, in our model we assume forced convection, thus taking (Incropera and De Witt, 1985; Leigh et al., 2012):

$$Nu=\begin{cases}0.60Re^{1/2} & \text{for } Re\le10^4\\ 0.032Re^{4/5}+9.2 & \text{for } Re>10^4.\end{cases} \tag{2}$$

The radiative flux is (e.g., Nobel, 2005; Leigh et al., 2012):

$$Q_{rad}=a_V S_0\cos(\phi_S)\left(|\sin(\phi^{(i)}-\phi_S)|+r\right)+a_{IR}\sigma\left(T_{sky}^4+T_{surr}^4\right)-2e_{IR}\sigma\left(T_l^{(i)}\right)^4, \tag{3}$$

where the three terms on the right-hand side correspond respectively to the direct and reflected solar radiation on the leaf, the infrared radiation absorbed by the leaf, and the infrared radiation emitted by the leaf. Here, a_V and a_{IR} are respectively the leaf absorptances at visible and infrared wavelengths respectively, r is the reflectance of the surroundings, S_0 is the direct solar radiation at full zenithal sunlight, $\phi^{(i)}$ is the leaf inclination angle, ϕ_S is the solar azimuthal angle, with $\phi_S=0$ if the sun is at the zenith and $\phi_S=\pi/2$ if it is at the horizon, σ is the Stefan–Boltzmann constant ($\sigma=5.67\times10^{-8}$ W m^{-2} K^{-4}), T_{sky} and T_{surr} are respectively the effective temperatures of the sky and the surroundings, and e_{IR} is the leaf emissivity at infrared wavelengths. Eq. (3) assumes that the leaf is at some height above ground, and thus that the direct solar radiation is incident only on the top surface of the leaf, the reflected and diffusive visible and infrared radiations only on the bottom surface, and that the emitted infrared radiation emanates from both leaf surfaces, hence the factor of 2 in front of the last term (Leigh et al., 2012). In this paper we represent the direct solar radiation by the first term in Eq. (3) by assuming an idealized two-dimensional tree oriented so that the sun trajectory and the deformed petiole shape are both contained on the plane of symmetry of the leaves. We also disregard self-shading effects within the tree crown.

Since $T_l^{(i)}$ is usually close to T_a, in our derivation we linearize Eq. (3) by approximating

$$2e_{IR}\left(T_l^{(i)}\right)^4\approx2e_{IR}T_a^4+8e_{IR}T_a^3(T_l^{(i)}-T_a). \tag{4}$$

In order to simplify the model's calculations, we only keep the leading-order terms in the infrared radiation term. The conserved terms are all of leading-order, since the typical magnitude of $2e_{IR}T_a^4$ is comparable to the magnitude of the direct radiation, $a_V S_0$, and the magnitude of $8e_{IR}T_a^3(T_l^{(i)}-T_a)$ is comparable to that of $\alpha(T_a-T_l^{(i)})$ in Eq. (1). Terms of order $(T_l^{(i)}-T_a)^2$ can however be neglected in our leading-order approximation.

We can estimate the typical time scale involved in Eq. (1) by balancing the time-dependent term on the left-hand side with the typical magnitude of the net radiation, on the order of 10–1000 W/m^2. Assuming $t_l\approx0.5$ mm, $C_l\approx2.5$ MJ m^{-2} K^{-1} (Leigh et al., 2012), and a typical leaf temperature variation $\Delta T_l^{(i)}\approx10$ K, we obtain a typical time scale on the order of seconds, which is much smaller than our time scales of interest (hours to days). We can thus assume steady state ($dT_l^{(i)}/dt=0$). With our approximation given by Eq. (4), Eq. (1) then yields the

following approximate expression for the leaf temperature, which we have derived by assuming a two-dimensional tree:

$$T_l^{(i)} = T_a + \frac{1}{\alpha + 8e_{IR}\sigma T_a^3}\left[a_V S_0 \cos(\phi_S)\left(|\sin(\phi^{(i)} - \phi_S)| + r\right) - \frac{L\rho q_{T,l}^{(i)}}{A_l} + Q\right], \quad (5)$$

where $Q \equiv a_{IR}\sigma(T_{sky}^4 + T_{surr}^4) - 2e_{IR}\sigma T_a^4$ takes a constant value in our calculation.

2.2. Transpiration in the leaf

Following Buckley (2005), we assume that the transpiration flux from the leaf can be written as the product of the stomatal conductance, g_s (mol m^{-2} s^{-1}), and the humidity difference between leaf i and the air, $w_l^{(i)} - w_a$ (mol H_2O/mol air). Thus, the transpiration flux through leaf i is

$$q_{T,l}^{(i)} = V_{mw} A_l g_s \left(w_l^{(i)} - w_a\right), \quad (6)$$

where $V_{mw} = 18 \times 10^{-6}$ m^3/mol is the molar volume of water. Note that $w_a = H\, w_{sat}(T_a)$, where H is the relative air humidity and $w_{sat}(T_a)$ is the water vapor saturation humidity at air temperature. We also assume that the humidity in the leaf corresponds to water vapor saturation at the leaf temperature, i.e., $w_l^{(i)} = w_{sat}(T = T_l^{(i)})$. The relationship between water saturation and temperature (e.g., Nobel, 2005) can be fitted by a quadratic polynomial:

$$w_l \approx a_T T_l^2 - b_T T_l + c_T, \quad (7)$$

where, with T_l in K and w_l in mol H_2O/mol air, the dimensional coefficients are $a_T = 6.2398 \times 10^{-5}$, $b_T = 3.5216 \times 10^{-2}$, and $c_T = 4.9830$. This fitting has been obtained for $288.15 \le T_l \le 323.15$ K (15–50 °C), with a maximum relative error in w_l of 18%. In the calculation that follows, it will be more convenient to use a polynomial fitting of T_l as a function of w_l:

$$T_l \approx -a w_l^2 + b w_l + c. \quad (8)$$

By expressing T_l in K and w_l in mol H_2O/mol air, the dimensional values a=2966, b=722, and c=277 yield a fitting with a maximum error of 2.2 K in the range $0.012 \le w_l \le 0.12$.

The stomatal conductance is assumed to depend on the leaf water potential through a logistic function similar to the one proposed by Tuzet et al., 2003:

$$g_s = g_0 + g_1 \frac{1}{1 + e^{s(\Psi_r - \Psi_l)}}, \quad (9)$$

where Ψ_l is the leaf water potential (Pa) and Ψ_r is a reference potential. Eq. (9) indicates that at high water potential ($\Psi_l \gg \Psi_r$), stomatal conductance is equal to $g_0 + g_1$ ("open stomata"), whereas at low water potential ($\Psi_l \ll 0$) stomatal conductance is equal to g_0 ("closed stomata"). The sensitivity parameter s (Pa^{-1}) controls the abruptness of the transition between the "open" and "closed" states. By modulating the value of Ψ_r we can model anisohydric behavior ($\Psi_l \gg \Psi_r$) or isohydric behavior ($\Psi_l \sim \Psi_r$).

2.3. Hydrodynamics of the xylem

We assume that the flow rate in the xylem is set by the transpiration rate in the leaves, $Q_T = \sum_{i=1}^{N} q_{T,l}^{(i)}$, where N is the number of leaves in the tree. We neglect phloem flow of limited effect on the physical couplings discussed in this paper We disregard changes in water storage in the soil surrounding the roots, which should be taken into account when describing the tree response over time scales of several days to weeks (Tuzet and Perrier, 2008), whereas here we focus on the tree response to water stress over a shorter time scale of hours to days. We also disregard water storage in the plant. Thus, the results presented here describe water stress upon exhaustion of available reserves in tissue storage. With these simplifications, head loss between the soil and the petiole yields:

$$\Psi_l = \Psi_s - R_x Q_T, \quad (10)$$

where Ψ_s is the water potential of the soil and R_x is the global hydraulic resistance of the soil, roots, and xylem. Ψ_l is assumed to represent both leaf and petiole water potential, thus disregarding head losses through the petiole and leaf veins. If the hydraulic resistance of the petiole was significant, and without changing our model's conclusions, we could readily reinterpret our equations by considering that petiole hydraulic resistance is included in R_x and that we express the petiole rigidity (Eq. (14)) in terms of the hydraulic pressure at the leaf. Without matrix wetting effects, the leaf water potential is

$$\Psi_l = p_t - \Pi + \rho g h, \quad (11)$$

where p_t is the turgor pressure (relative to the atmospheric pressure), Π is the osmotic pressure, here assumed constant, and h is the height of the tree. Combining Eqs. (10) and (11) yields:

$$p_t = \Psi_s - R_x Q_T - \rho g h + \Pi. \quad (12)$$

2.4. Leaf inclination

We describe the inclination of a leaf by applying the expression deduced by Tadrist et al. (2014) to the case of a leaf deflected by its own weight (we neglect the wind effect on leaf inclination):

$$\phi^{(i)} = \left[\frac{|\theta^{(i)}| + \pi E_G}{1 + E_G}\right] \mathrm{sgn}(\theta^{(i)}), \quad (13)$$

where $\phi^{(i)}$ is the angle of leaf i with the vertical direction ($\phi^{(i)} = 0$ for a leaf pointing towards the sky and $\phi^{(i)} = \pi/2$ for a horizontal leaf, see Fig. 1); $\theta^{(i)}$ is the angle of the petiole at the branching with the vertical direction; and $E_G = \Lambda L m g/(EI)$ is the elasto-gravity number, with Λ being the arm of the leaf's weight, mg, L the length of the petiole, and EI the bending rigidity of the petiole. Eq. (13) is an approximate solution of the elastic beam equation assuming $\Lambda/L \ll 1$ and $\psi \approx \pi$; the reader is referred to Tadrist et al. (2014) for details (in practice, Eq. (13) remains reasonably accurate for $\psi > \pi/3$). The elastic modulus E depends on turgor pressure (Nilsson et al., 1958; Niklas and Spatz, 2012). Niklas and Spatz (2012) considered a spherical cell and suggested a relationship that can be written in the form $E = E_0 + \gamma p_t$, where E_0 and γ are constants. Without loss of generality we can assume $E_0 = 0$, since we are free to redefine the zero absolute pressure at the point of complete wilting (E=0). Thus, if $p_t > 0$, we can write:

$$E_G = \frac{p_t^{(0)}}{p_t}, \quad (14)$$

where $p_t^{(0)}$ is the turgor pressure that yields $E_G = 1$. Note that, if $p_t \le 0$, then $\phi = \pi$ and the leaf points vertically downwards (complete wilting).

Combining Eqs. (13) and (14) leads to:

$$\phi^{(i)} = \begin{cases} \left[\dfrac{|\theta^{(i)}|\, p_t + \pi p_t^{(0)}}{p_t + p_t^{(0)}}\right] \mathrm{sgn}(\theta^{(i)}) & \text{if } p_t > 0, \\ \pi\, \mathrm{sgn}(\theta^{(i)}) & \text{if } p_t \le 0. \end{cases} \quad (15)$$

2.5. Nondimensionalization

The problem is governed by Eqs. (5), (6) (12) and (15). The four unknowns are the leaf-to-air temperature difference, $\Delta T^{(i)} = T_l^{(i)} - T_a$, the leaf transpiration flux, $q_{T,l}^{(i)}$, the turgor pressure, p_t, and the leaf inclination angle, $\phi^{(i)}$. Moreover, Eqs. (5) and (6) are coupled via the auxiliary variable $\Delta w^{(i)} = w_l^{(i)} - w_a$ (the leaf-to-air humidity difference), which is related to $\Delta T^{(i)}$ through Eq. (7).

To nondimensionalize the problem, we choose $p_t^{(0)}$ (the turgor pressure yielding $E_G = 1$) as the unit pressure, $\Delta T_0 \equiv a_V S_0/(\alpha + 8 e_{IR}\sigma T_a^3)$ (the leaf-to-air temperature difference due to direct solar radiation) as the unit temperature difference, $\Delta w_0 \equiv w_{sat}(T_l = T_a + \Delta T_0) - w_a$ (the leaf-to-air humidity difference corresponding to the unit temperature difference ΔT_0) as the unit humidity difference. We thus define the following nondimensional variables:

$$\Delta\hat{T}^{(i)} \equiv \frac{\Delta T^{(i)}}{\Delta T_0} \tag{16}$$

$$\Delta\hat{w}^{(i)} \equiv \frac{\Delta w^{(i)}}{\Delta w_0} \tag{17}$$

$$\hat{q}_{T,l}^{(i)} \equiv \frac{q_{T,l}^{(i)}}{N V_{mw} A_l g_1 \Delta w_0} \tag{18}$$

$$\hat{p}_t \equiv \frac{p_t}{p_t^{(0)}}, \tag{19}$$

plus the variable $\phi^{(i)}$, which is already nondimensional.

The normalized governing equations are:

$$\Delta\hat{T}^{(i)} = |\sin(\phi^{(i)} - \phi_S)| \cos\phi_S + r\cos\phi_S + \hat{Q} - C_L \hat{g}\Delta\hat{w}^{(i)} \tag{20}$$

$$\hat{q}_T = \frac{\hat{g}\sum_{i=1}^{N}\Delta\hat{w}^{(i)}}{N} \tag{21}$$

$$\hat{p}_t = \hat{\Psi}_{eff} - C_g \hat{q}_T \tag{22}$$

$$\phi^{(i)} = \begin{cases} \left[\dfrac{\pi + |\theta^{(i)}|\hat{p}_t}{1+\hat{p}_t}\right]\mathrm{sgn}(\theta^{(i)}) & \text{if } \hat{p}_t > 0 \\ \pi\,\mathrm{sgn}(\theta^{(i)}) & \text{if } \hat{p}_t \le 0. \end{cases} \tag{23}$$

The normalized equations contain the following nondimensional coefficients:

$$\hat{\Psi}_{eff} \equiv \frac{\Psi_s + \Pi - \rho g h}{p_t^{(0)}} \tag{24}$$

$$\hat{Q} \equiv \frac{Q}{a_V S_0} \tag{25}$$

$$C_g \equiv \frac{R_X N V_{mw} A_l g_1 \Delta w_0}{p_t^{(0)}} \tag{26}$$

$$C_L \equiv \frac{L\rho V_{mw} g_1 \Delta w_0}{a_V S_0}. \tag{27}$$

The meaning of these four nondimensional coefficients is the following. $\hat{\Psi}_{eff}$ represents the available soil water potential, relative to the pressure needed to keep the petiole turgid. $\hat{Q}$ represents the ratio of indirect radiation on the leaf (independent of its inclination) to the direct radiation (dependent on the leaf and sun inclinations). C_g represents the importance of water potential loss due to flow along the xylem, relative again to the pressure needed to keep the petiole turgid; this coefficient is directly proportional to the stomatal conductance g_s. C_L represents the importance of the evaporation term in the energy balance, compared to the solar radiation term. Considering typical parameter values for a tree obtained from the literature (see Table 1), one deduces that C_L, $\hat{\Psi}$, $\hat{Q}$, and C_g are all of order 1 (larger than 0.1 and smaller than 10). This result indicates that all physical phenomena accounted for by the model are of comparable quantitative importance. Thus, for a tree characterized by the parameter values in Table 1, none of these physical phenomena can be neglected.

An auxiliary equation, derived from Eq. (8), relates $\Delta\hat{T}^{(i)}$ with $\Delta\hat{w}^{(i)}$:

$$\Delta\hat{T}^{(i)} \approx -\hat{a}(\Delta\hat{w}^{(i)})^2 + \hat{b}\Delta\hat{w}^{(i)} - \hat{c}, \tag{28}$$

with $\hat{a} = a(\Delta w_0)^2/\Delta T_0$, $\hat{b} = (b - 2aw_a)\Delta w_0/\Delta T_0$, and $\hat{c} = [bw_a(1 - H)/H - aw_a^2(1-H^2)/H^2]/\Delta T_0$, where $H = w_a/w_{sat}(T = T_a)$ is the fraction of saturation humidity in the air.

Finally, the stomatal conductance (Eq. (9)) is normalized to yield

$$\hat{g} = G_0 + \frac{1}{1 + e^{S(\hat{\Psi}_r - \hat{p}_t)}}, \tag{29}$$

where $\hat{g} \equiv g_s/g_1$, $G_0 \equiv g_0/g_1$, $S \equiv s p_t^{(0)}$, and $\hat{\Psi}_r \equiv (\Psi_r + \Pi)/p_t^{(0)}$.

The problem can be reduced to a system of equations for the variables $\hat{p}_t$ and $\phi^{(i)}$:

$$\hat{p}_t = \hat{\Psi}_{eff} - \frac{C_g\hat{g}}{\sqrt{\hat{a}}}\left[\alpha_0 - \frac{1}{N}\sum_{i=1}^{N}\sqrt{\alpha_0^2 - (\hat{c}+\hat{Q}) - \cos(\phi_S)(|\sin(\phi^{(i)} - \phi_S)| + r)}\right] \tag{30}$$

$$\phi^{(i)} = \begin{cases} \left[\dfrac{\pi + |\theta^{(i)}|\hat{p}_t}{1+\hat{p}_t}\right]\mathrm{sgn}(\theta^{(i)}) & \text{if } \hat{p}_t > 0 \\ \pi\,\mathrm{sgn}(\theta^{(i)}) & \text{if } \hat{p}_t \le 0, \end{cases} \tag{31}$$

where $\alpha_0 \equiv (\hat{b} + C_L)/(2\sqrt{\hat{a}})$, and $\hat{g}$ is given by Eq. (29).

2.6. Branch and leaf inclination angle distributions

In the following we will consider two representations of the tree geometry. First, we will consider a uniform foliage model (Fig. 1A) where all N leaves of the tree have identical inclinations (i.e., same $\theta^{(i)}$ and thus same $\phi^{(i)}$). In this uniform foliage model, Eqs. (30) and (31) reduce to a system of two equations with two unknowns, $\hat{p}_t$ and ϕ.

Second, we will consider a distributed foliage model (Fig. 1B), where a single trunk is connected to N leaves with different inclinations. Such a geometry is characterized by the branch inclination angle distribution (BIAD). Strictly speaking, our model tree does not have branches, and the BIAD actually refers to the branching angle at which the petiole stems from the trunk. The BIAD can be represented by a polar plot (brown dashed curve in the inset of Fig. 1B), where the distance from the origin to the curve, measured along a given radius, is proportional to f_θ, the probability that a given tree branch is oriented in the direction of that radius. As discussed by Tadrist et al. (2014), a realistic description of a tree BIAD is provided by a Gaussian distribution of the form:

$$f_\theta(\theta) = A_\theta e^{-(|\theta| - \mu_\theta)^2/(2\sigma_\theta^2)}, \tag{32}$$

where μ_θ and σ_θ are the mean and standard deviation, and A_θ is a constant. As studied by Tadrist et al. (2014), petiole flexibility and leaf weight cause leaves to have a larger inclination than branches do. In a distributed foliage model, leaf geometry is characterized by a leaf inclination angle distribution (LIAD, green solid curve in the inset of Fig. 1B) different than the BIAD. If the BIAD is known, one can apply Eq. (31) to the different leaves to deduce the LIAD. In this way, the BIAD in Eq. (32) yields the following LIAD:

$$f_\phi(\phi) = \begin{cases} A_\phi e^{-(|\phi| - m_\theta)^2/(2s_\phi^2)} & \text{if } \phi_{min} \le |\phi| \le \pi \\ 0 & \text{otherwise,} \end{cases} \tag{33}$$

where $m_\phi \equiv (\pi+\hat{p}_t\,\mu_\theta)/(1+\hat{p}_t)$, $s_\phi \equiv \sigma_\theta\,\hat{p}_t/(1+\hat{p}_t)$, $\phi_{\min} \equiv \pi/(1+\hat{p}_t)$, and

$$A_\phi = \frac{1}{s_\phi}\sqrt{\frac{2}{\pi}}\frac{1}{\left[\operatorname{erf}\left(\frac{\pi-\mu_\theta}{\sigma_\theta\sqrt{2}}\right)+\operatorname{erf}\left(\frac{\mu_\theta}{\sigma_\theta\sqrt{2}}\right)\right]}. \tag{34}$$

3. Results and discussion

We start this part by discussing the results obtained for the uniform foliage model. In Section 3.1 we study how petiole flexibility affects the minimal pressure attained in a tree and thus the risk of cavitation. Cavitation is a progressive phenomenon, where xylem conductance decreases progressively with decreasing xylem pressure, as described by the so-called xylem vulnerability curve (Cochard, 2006). Here we do not consider the tree vulnerability curve, but rather we describe cavitation by the pressure threshold for the onset of xylem embolism. In Section 3.2 we investigate the impact of parameter uncertainty on the results by performing a Sobol sensitivity analysis of the uniform foliage model. Next, in Section 3.3, we repeat the study of petiole flexibility effects in the more realistic distributed foliage model. In Section 3.4 we introduce active stomatal closure to model isohydric and anisohydric tree strategies. For a specific water stress level, we study how these two strategies, combined with petiole flexibility, affect photosynthesis and cavitation. Finally, in Section 3.5 we investigate a range of water stress levels and a range of sensitivities of petiole flexibility to changes in turgor pressure, in order to construct a phase diagram of tree responses to water stress. The phase diagram shows the efficacy of different tree strategies against the risks of cavitation and carbon starvation. The results of this last subsection demonstrate that turgidity-dependent petiole flexibility increases a tree's water use efficiency under water stress.

3.1. Uniform foliage model

Here we study the uniform foliage model, which consists of N identical leaves, and we assume the stomatal conductance g_s to remain constant. Fig. 2 shows the response of the uniform foliage model to water stress, here represented by a reduction of the soil water potential (a reduction of Ψ_s or, in nondimensional terms, a reduction of $\hat{\Psi}_{\text{eff}}$). The sun is either at the zenith ($\phi_S = 0$, Fig. 2A and B) or at an intermediate inclination ($\phi_S = \pi/4$, Fig. 2C and D). Each plot represents four cases, for which the tree petioles are either flexible (solid lines) or rigid (dashed and dotted lines), and the branch inclination is either $\theta = 0$ (blue lines) or $\theta = \pi/2$ (red lines). The figure shows that leaf wilting due to petiole flexibility significantly affects the minimal pressure attained in the xylem, $\hat{p}_t$, and thus the risk for the tree to cavitate. For example, for $\theta = \pi/2$ and $\phi_S = 0$, petiole flexibility protects the tree from cavitation, since for a given $\hat{\psi}_{\text{eff}}$ the pressure attained by a flexible tree (solid red line in Fig. 2A) is larger than the pressure attained by a rigid tree (dashed red line). In contrast, the effect of petiole flexibility is the opposite for an upward-pointing branch ($\theta = 0$), since in this case flexibility increases the risk of cavitation. These opposite effects can readily be interpreted as follows. In the case of a

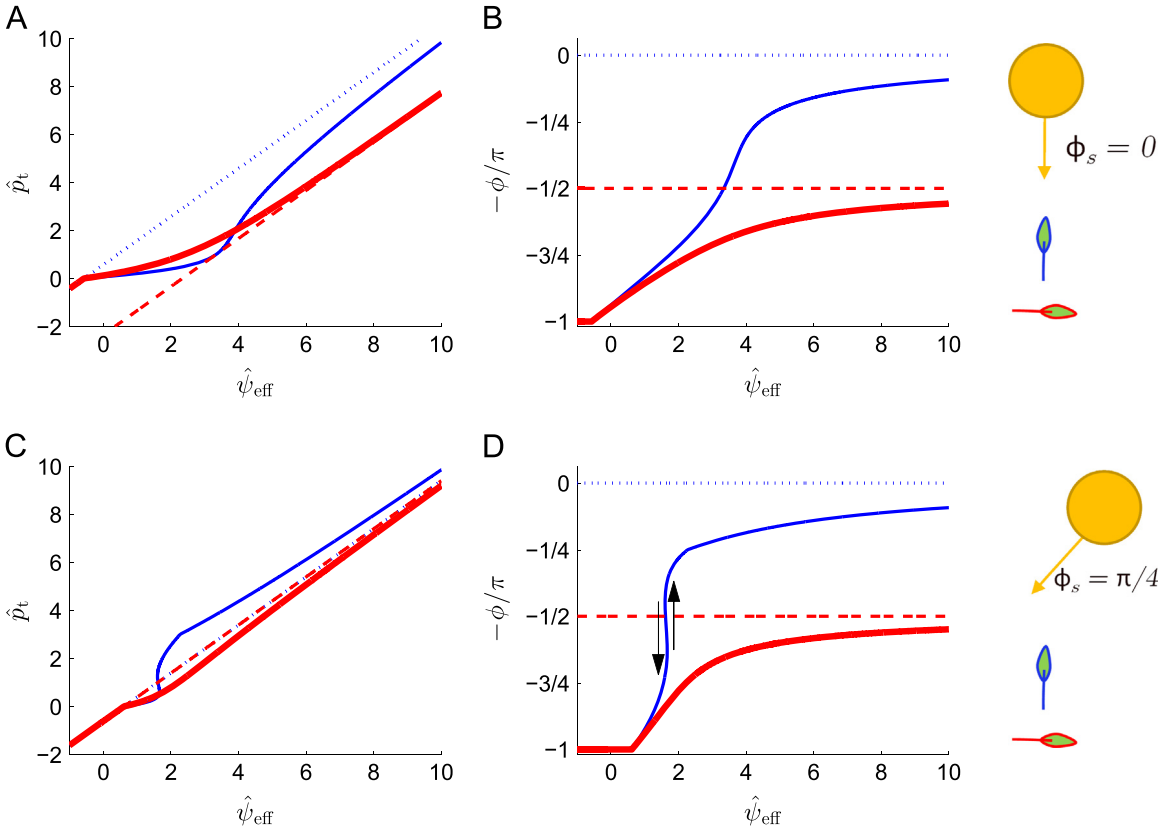

Fig. 2. Response to water stress of the uniform foliage model. Parameter values correspond to reference values in Table 1, with the stomata assumed always open (constant g_s). (A) and (C) Nondimensional minimal pressure attained in the xylem ($\hat{p}_t$) versus soil water content ($\hat{\psi}_{\text{eff}}$). (B) and (D) Corresponding variation of the leaf inclination angle, ϕ. The upper plots ((A) and (B)) correspond to a zenithal sun ($\phi_s = 0$) and the lower plots ((C) and D) correspond to $\phi_s = \pi/4$. The thin solid blue lines correspond to a flexible and initially upward-pointing leaf ($\theta = 0$), and the dotted blue lines to a rigid leaf also with $\theta = 0$. The thick solid red lines correspond to a flexible and initially horizontal leaf ($\theta = \pi/2$), and the dashed red lines to a rigid leaf also with $\theta = \pi/2$. (For interpretation of the references to color in this figure caption, the reader is referred to the web version of this paper.)

horizontal branch ($\theta = \pi/2$), flexibility reduces the sun irradiation on the leaf. Thus, transpiration through the leaf and head loss along the xylem decrease, and the minimal pressure attained in the xylem is less pronounced than for a rigid petiole. For an upward-pointing branch ($\theta = 0$), however, flexibility increases sun irradiation onto the leaf, thus increasing transpiration and making the minimal xylem pressure more negative.

Fig. 2B and D shows the evolution of the leaf inclination angle as a function of water stress. Interestingly, the leaf inclination angle can increase steeply for a small reduction of soil water content, for example for the case of $\theta = 0$ and $\phi_S = \pi/4$ (solid blue line in Fig. 2B and D). It is noted that the curve has a slight S shape, which is indicative of hysteresis (represented by the black arrows): if the soil is drying, the water content at which the leaf wilts is $\hat{\Psi}_{\text{eff}} \approx 1.60$, smaller than the soil water content required for the leaf to recover turgidity upon soil rehydration ($\hat{\Psi}_{\text{eff}} \approx 1.66$). Physically, this hysteresis loop is due to the leaf avoiding an inclination normal to solar irradiation. Hysteretic effects between dehydration and rehydration have been experimentally observed in plants and attributed to elastic hysteresis in cell tissue response to turgor pressure (Murphy and Ortega, 1996). Here, we identify a new mechanism of dehydration–rehydration hysteresis, arising from an interplay between the leaf and the sun inclination angles.

3.2. Sensitivity analysis

We next consider how the uncertainty in the model parameters may impact the model's results discussed above. Fig. 3 shows the result of a Sobol sensitivity analysis (e.g., Saltelli et al., 2004) of the uniform foliage model, in terms of the dimensional parameters. The goal of this analysis is to determine how the variance in the calculated turgor pressure, p_t, can be attributed to the variances of the model's dimensional parameters (listed along the abscissa of Fig. 3). We perform a Monte Carlo experiment consisting of 10^4 realizations, in which the model parameters take random values that are uniformly distributed within their ranges of variation (Table 1). Fig. 3 shows two types of variance decomposition indices: first-order Sobol indices (light blue bars in the figure), which represent the fraction of the variance of the output due to the variation of a single parameter (but averaged over variations in all the other parameters); and total-order Sobol indices (dark red bars in the figure), which represent the fraction of the variance of the output due to the variation of a given parameter, alone and in interaction with other input variables. As a consequence of their definitions, the sum of first-order Sobol indices (rightmost light blue bar) is smaller than 1, since it disregards the fraction of the variances resulting from their interactions, whereas the sum of total-order indices (rightmost dark red bar, truncated) is larger than 1, since the interaction terms are counted multiple times. Sobol indices are calculated by applying the modified Homma–Saltelli method proposed by Wu et al. (2012). The figure indicates that the model is highly nonlinear, since the variance is dominated by parameter interactions (i.e., the total Sobol indices are significantly larger than the first-order indices). The model is particularly sensitive to leaf and sun inclinations, as it is intuitively expected, as well as to heat exchange parameters (a_V, S_0, T_{sky}, T_{surr}), to certain hydraulic parameters (g_s and R_X), and to petiole flexibility ($p_t^{(0)}$). The model is however rather insensitive to tree height (h) and to air humidity (H), within the assumed range of variability of these parameters. It is noted that the variance decomposition method of Sobol used here strictly applies to independent parameters only. Therefore, we should interpret these results as merely an indication on the mathematical dependence of the outputs on the parameters, since some of our parameters do not vary independently in reality. For example, hydraulic resistance R_X is expected to depend on tree height h, and thus the model is indirectly sensitive to h through its sensitivity to R_X.

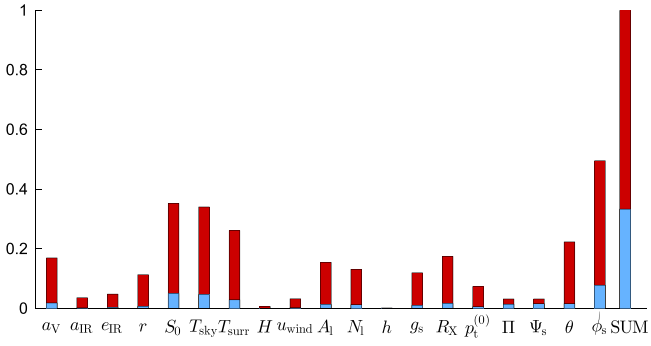

Fig. 3. Sobol sensitivity analysis of the uniform foliage model. The range of variability in the input parameters is listed in Table 1. The light blue bars correspond to first-order Sobol indices and the dark red bars to total-order Sobol indices. The sum of total-order Sobol indices is 2.8 (note that the height of the corresponding bar is not fully shown in the figure, truncated at height 1). (For interpretation of the references to color in this figure caption, the reader is referred to the web version of this paper.)

3.3. Distributed foliage model

To represent a tree more realistically than the uniform foliage model does, we next account for the diversity of branch orientations, which we represent by a Gaussian branch inclination angle distribution (BIAD). We continue to assume that all leaf petioles are located at the upper end of a common xylem, and thus the value of p_t remains common to them all. Fig. 4A shows the nondimensional turgor pressure as a function of the nondimensional soil water content, assuming a zenithal sun ($\phi_S = 0$) and a BIAD of mean $\mu_\theta = \pi/4$ and standard deviation $\sigma_\theta = \pi/8$, which are values representative of real trees (Tadrist et al., 2014). The solid line in the figure represents the response of a flexible tree. The dashed line represents a rigid tree for which the leaf inclination angle

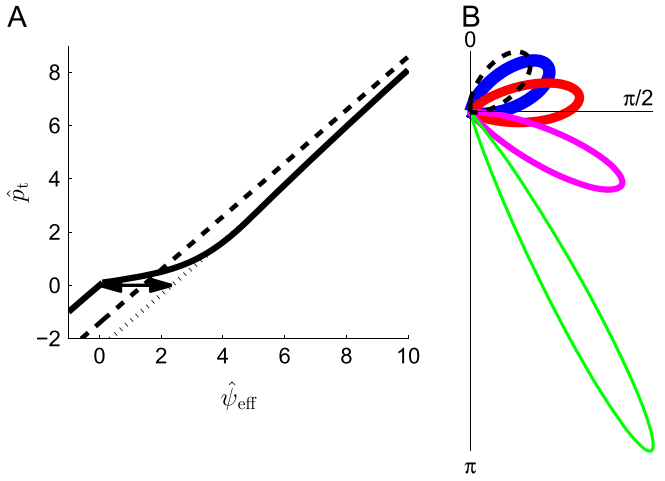

Fig. 4. Response to water stress of a tree with normally distributed branch inclination angles ($\mu_\theta = \pi/4$, $\sigma_\theta = \pi/8$). Parameter values correspond to reference values in Table 1, with the stomata assumed always open (constant g_s) and the sun at the zenith ($\phi_S = 0$). (A) Nondimensional minimal pressure attained in the xylem ($\hat{p}_t$) versus soil water content ($\hat{\psi}_{eff}$) for flexible petioles (solid line) or rigid petioles (dashed line). The dotted line indicates a rigid tree that keeps the leaf inclination angles corresponding to $\hat{\psi}_{eff} = 5$, a well-watered condition. The double-pointing arrow indicates the protection against water stress due to petiole flexibility. (B) Polar representation of the evolution of the leaf inclination angle distribution with increasing water stress. The dashed black curve corresponds to an infinite $\hat{\psi}_{eff}$. The thickest blue line, thick red line, thin magenta line, and thinnest green line correspond respectively to $\hat{\psi}_{eff} = 10$, 5, 3, and 1. (For interpretation of the references to color in this figure caption, the reader is referred to the web version of this paper.)

distribution (LIAD) is identical to the BIAD. Thus, the solid line and the dashed line are asymptotically identical as $\hat{\Psi}_{\text{eff}} \to \infty$. The dotted line represents a rigid tree whose LIAD is identical to that of the flexible tree at $\hat{\Psi}_{\text{eff}} = 0$, which dimensionally corresponds to a well watered condition ($\Psi_s = 0.1$ MPa). Thus, the gap between the dotted and the solid lines (double-pointing arrow) measures the protection from cavitation by petiole flexibility. In dimensional terms, this protection by flexibility corresponds to a reduction in the soil water potential for tree cavitation of about 0.5 MPa. Fig. 4B shows the evolution of the LIAD with decreasing soil water content. It illustrates how, as the leaves wilt, the LIAD's standard deviation decreases. Indeed, at complete wilting, all leaves reach the same inclination ($\phi = \pi$).

3.4. Effect of water stress on photosynthesis

At this point we introduce two paradigms of tree response to water stress: a tree can let leaf water potential fluctuate (anisohydric behavior) or it can regulate stomatal opening to keep a relatively constant leaf water potential (isohydric tree). To model these two idealized tree responses, and unlike the constant value of g_s assumed in the simulations above, in the following we consider that stomatal opening varies with leaf water potential, as described by Eq. (9). As discussed above, the choice of Ψ_r in Eq. (9) allows us to represent either anisohydric or isohydric behavior. Fig. 5 represents the variation of g_s for two different choices of Ψ_r, which in the following correspond to our model isohydric tree (blue line) and to our model anisohydric tree (red line). The gray region in Fig. 5 indicates the typical range of variation of soil water potential considered in the following. It is noted that only the isohydric tree significantly regulates stomatal opening over this range.

In what follows, we will investigate not only the risk of cavitation due to water stress, but also the effect of water stress on photosynthetic carbon assimilation. To compute carbon assimilation, we use the model of Farquhar et al. (1980). A summary of the model's equations is presented in Appendix A. For the sake of clarity, in the following the model results will be presented in dimensional form. In order to account for daily photosynthesis

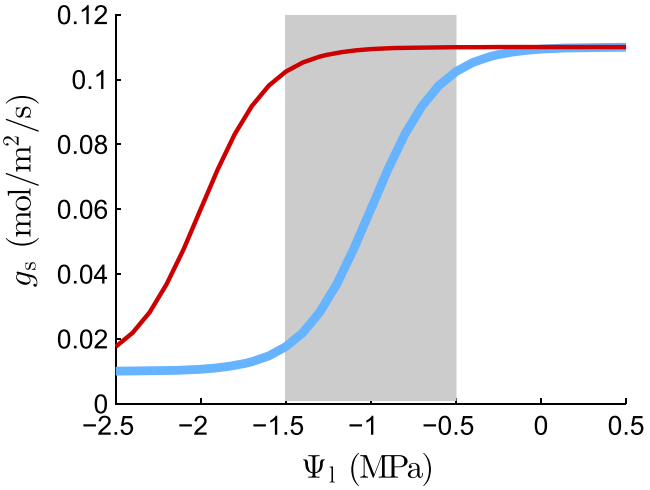

Fig. 5. Dependence of the stomatal conductance, g_s, on the leaf water potential, Ψ_l, for two stomatal parameter sets, that we call *isohydric* ($\Psi_r = -1$ MPa, thick light blue line) and *anisohydric* ($\Psi_r = -2$ MPa; thin dark red line). For both cases, the sensitivity parameter is taken as $s = 5 \times 10^{-6}$ Pa^{-1}, and the closed and open stomatal conductances as $g_0 = 0.01$ mol m^{-2} s^{-1} and $g_1 = 0.1$ mol m^{-2} s^{-1} respectively. The shaded gray region is indicative of the interval of leaf water potentials that are experienced during moderate water stress. (For interpretation of the references to color in this figure caption, the reader is referred to the web version of this paper.)

variations, we will now consider the evolution of the sun inclination over a given day. For simplicity, a light time of 12 h is assumed, and all parameters other than the sun inclination are assumed constant over the 24-h day.

Fig. 6 shows model results over a day assuming a BIAD of mean $\mu_\theta = \pi/4$ and standard deviation $\sigma_\theta = \pi/8$. The figure represents the cases of a isohydric and of an anisohydric tree (blue and red lines respectively), which have either flexible or rigid petioles (solid and dashed lines respectively). It is noted that, since we have not considered an explicit dependence of stomatal conductance on solar irradiation, our model does not reproduce stomatal closure at nighttime (see Fig. 6B). The isohydric tree responds to peak water stress at midday by closing the stomata (Fig. 6B), whereas the anisohydric tree responds by a more pronounced wilting (Fig. 6A). This result is consistent with observations of trees transiently wilting at midday, and rapidly recovering afterward (Chiariello et al., 1987). Fig. 6C shows that two strategies, stomatal control in isohydric trees and flexibility in anisohydric trees, are equally effective in limiting the minimal xylem pressure and thus the risk of cavitation, whereas the flexibility strategy of anisohydric trees is more efficient in terms of photosynthetic assimilation, as shown in Fig. 6D. The reader may find surprising that, in the isohydric case, the flexible tree attains a slightly lower pressure than the rigid tree (solid and dashed light blue lines in Fig. 6B). The reason is that in this example we chose $\mu_\theta = \pi/4$ which, due to leaf weight, renders the leaf inclinations of the flexible tree closer to $\pi/2$ than for the rigid tree, and thus more exposed to solar irradiation. This latter effect is of limited quantitative importance, since it does not affect the minimal pressure attained at midday, critical for cavitation, and moreover it remains small when compared to the other effects described above. In conclusion, importantly, our model results indicate that petiole flexibility offers a useful mechanism of tree protection against water stress. The efficiency of this protective mechanism is comparable to that attained by active control of stomatal opening.

3.5. Effect of water use strategies on the risks of cavitation and carbon starvation

In this final results section, we conduct a more systematic exploration of the efficiency of protection against water stress provided by turgidity-dependent petiole flexibility. In essence, the results discussed in what follows show that, under conditions of water stress, turgidity-dependent flexible petioles systematically provide higher water use efficiency than rigid petioles, as illustrated by the rapid raising of the flexible-petiole solid curves in Fig. 8 as compared with the sensibly flatter rigid-petiole dashed curves in the same figure. Moreover, due to the biochemistry of C_3 photosynthesis, a well-tuned flexible-petiole leaf can yield a larger carbon assimilation than a rigid horizontal leaf. This result is graphically represented by the solid color lines in Fig. 7B overtaking the daily CO_2 assimilation of the dashed black line, which represents the rigid horizontal leaf. In the remaining of this section we discuss these last results in more detail.

In Fig. 6, we considered only one particular value of petiole flexibility ($p_t^{(0)} = 10^4$ Pa) and of soil water potential ($\psi_s = -0.75$ MPa). In Fig. 7, we explore the response of an isohydric tree (plot A) and of an anisohydric tree (plot B) to a systematic variation of these two parameters, $p_t^{(0)}$ and ψ_s. In the phase diagrams of Fig. 7, the tree state is represented by its daily photosynthetic assimilation (horizontal axis) and by the minimal pressure attained at the xylem over the day (vertical axis), thus quantifying the two main water stress risks. Thin solid lines of different colors correspond to different tree flexibilities; more precisely, the parameter that is varied between different color

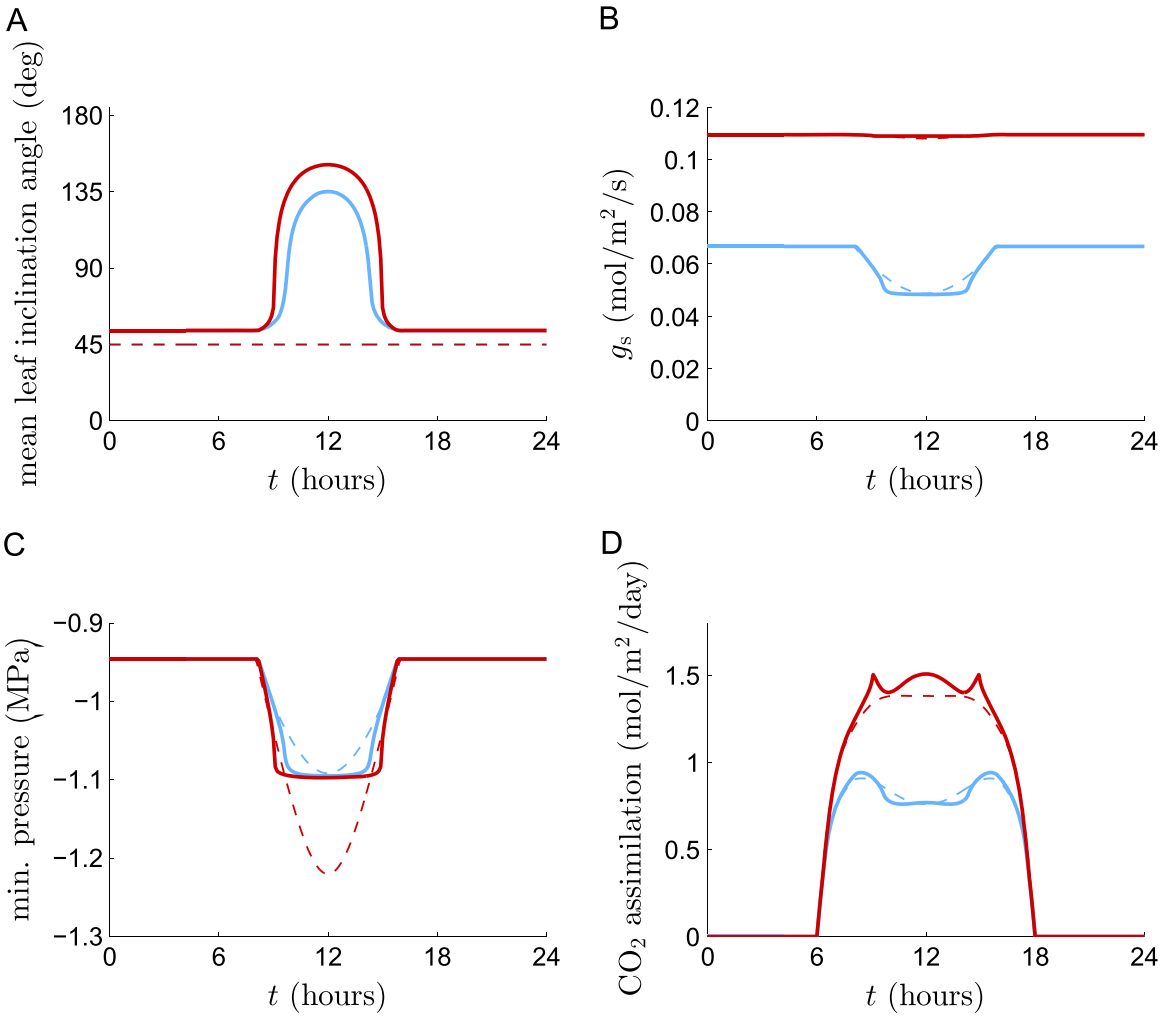

Fig. 6. Daily variation of the mean leaf inclination angle (A), the stomatal conductance (B), the minimal pressure attained in the xylem ((C)), and the photosynthetic CO_2 assimilation ((D)). The light blue and dark red lines correspond respectively to the *isohydric* and *anisohydric* cases, as defined in Fig. 5. The solid lines correspond to flexible petioles ($p_t^{(0)} = 10^4$ Pa) and the dashed lines to infinitely rigid petioles ($p_t^{(0)} \to \infty$). Computations are run for a BIAD of mean $\mu_\theta = \pi/4$ and standard deviation $\sigma_\theta = \pi/8$. The soil water potential is $\psi_s = -0.75$ MPa and the other parameters take their reference values in Table 1. (For interpretation of the references to color in this figure caption, the reader is referred to the web version of this paper.)

lines is $p_t^{(0)}$, which is inversely proportional to the slope of variation of Young's modulus with turgor pressure (see Eq. (14)). Three limit cases are also represented: an infinitely rigid tree (thick dashed red line), an infinitely flexible tree (thick dashed blue line), and an infinitely rigid tree where all leaves remain horizontal (thick dashed black line). Each curve represents the trajectory of the tree in the phase space as the water stress becomes more significant (i.e., as Ψ_s decreases). Isolines of water stress are represented by thin dashed black lines.

The most obvious difference between plots A and B in Fig. 7 is that water stress significantly reduces photosynthetic assimilation in isohydric trees (plot A), but not in anisohydric trees (plot B). In both plots, as we start reducing the flexibility from the infinitely rigid case (thick dashed red line), the trajectories move to the right. The isolines of water stress (consider for example the isoline $\Psi_s = 0$ in plot B) show that, whereas photosynthetic assimilation increases with flexibility, the minimal pressure becomes more pronounced. Thus, moderate flexibility (i.e., moving from point P, of zero flexibility, to point Q) increases photosynthetic assimilation but also the risk of cavitation. This effect of moderate flexibility corresponds to the LIAD evolving from upward-pointing to horizontal, the position at which photosynthetic assimilation but also transpiration are maximized (point R). If the flexibility continues to increase beyond the horizontal LIAD, the evolution of risks is reversed: photosynthetic assimilation decreases and minimal pressure becomes less pronounced (point S). Another remarkable feature of Fig. 7B is that tree flexibility may allow reaching a CO_2 assimilation rate larger than that of a perfectly horizontal rigid leaf. This counterintuitive result arises from our use of Farquhar et al.'s (1980) C_3 photosynthesis model. In this model, as well as in experiments with C_3 plants, electron transport reaches a maximum at around a leaf temperature of about 30 °C, and then decreases. Because petiole flexibility attenuates heating by leaf deflection at midday, a near-horizontal but flexible leaf can be more photosynthetically productive than a rigid horizontal leaf.

Fig. 8 shows water use efficiency (mass of CO_2 assimilated by the tree per unit mass of water loss by transpiration, WUE) for isohydric and anisohydric trees. The color coding is identical to that of Fig. 7. As compared to rigid trees (thick dashed lines), the WUE of flexible trees systematically increases under conditions of water stress (negative soil water potential). The figure shows that, in terms of WUE, petiole flexibility allows trees to more efficiently use water during drought. It is noted that, whereas the maximum instantaneous WUE predicted by our model is of the same order of magnitude as in real trees, the daily average WUE values reported in Fig. 8 are almost one order of magnitude higher than real values measured in trees (Nobel, 2005). This discrepancy is due to our model not accounting for stomatal closure that occurs overnight,

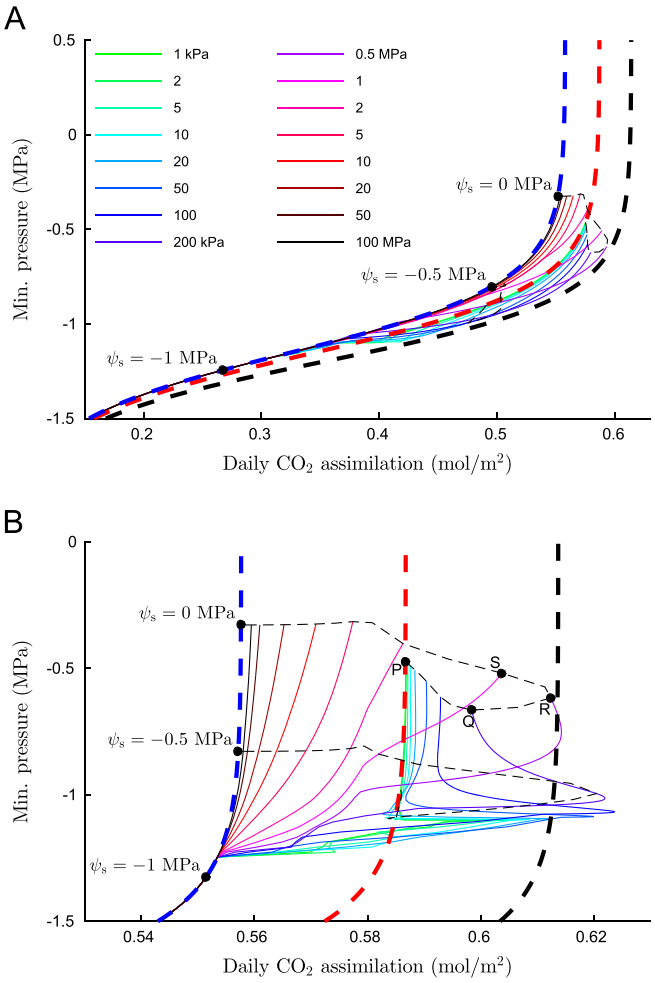

Fig. 7. Phase diagram of the daily CO_2 assimilation versus the minimal pressure reached in the xylem. Plots (A) and (B) correspond respectively to an *isohydric* and an *anisohydric* tree, as defined in Fig. 5. Different solid color lines correspond to different values of the reference petiole turgor pressure, $p_t^{(0)}$. Other than $p_t^{(0)}$, the reference parameter values in Table 1 are used. The BIAD's mean and standard deviations are $\mu_\theta = \pi/4$ and $\sigma_\theta = \pi/8$ respectively. The thick dashed red line corresponds to the infinitely rigid case ($p_t^{(0)} \to \infty$) and the thick dashed blue line to the infinitely flexible case ($p_t^{(0)} = 0$). The thick dashed black line corresponds to an infinitely rigid tree with all leaves oriented horizontally ($p_t^{(0)} \to \infty$, $\mu_\theta = \pi/2$, $\sigma_\theta = 0$). Thin dashed lines are isolines of soil water potential, ψ_s. (For interpretation of the references to color in this figure caption, the reader is referred to the web version of this paper.)

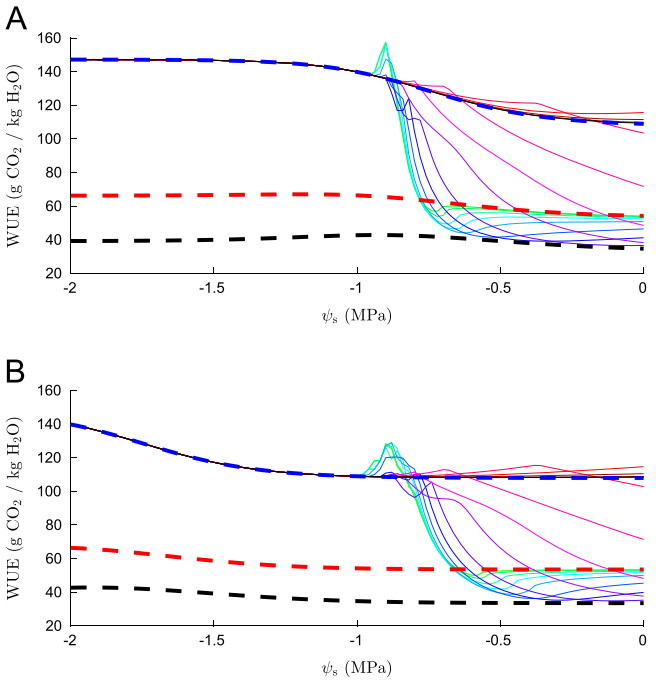

Fig. 8. Water use efficiency versus soil water potential. Plots (A) and (B) correspond respectively to an *isohydric* and an *anisohydric* tree, as defined in Fig. 5. Different solid color lines correspond to different values of the reference petiole turgor pressure (see color coding in Fig. 7). Other than $p_t^{(0)}$, the reference parameter values in Table 1 are used. The BIAD's mean and standard deviations are $\mu_\theta = \pi/4$, $\sigma_\theta = \pi/8$. The thick dashed red line corresponds to the infinitely rigid case ($p_t^{(0)} \to \infty$) and the thick dashed blue line to the infinitely flexible case ($p_t^{(0)} = 0$). The thick dashed black line corresponds to an infinitely rigid tree with all leaves oriented horizontally ($p_t^{(0)} \to \infty$, $\mu_\theta = \pi/2$, $\sigma_\theta = 0$). (For interpretation of the references to color in this figure caption, the reader is referred to the web version of this paper.)

as discussed above. This simplification of the model, that we have kept in order to focus on the role of flexibility, does not affect the qualitative conclusions about the effect of petiole flexibility on the WUE.

4. Conclusion

We have developed an analytical model of the coupling between heat exchange at the leaf, petiole mechanics, and xylem flow to study the role of wilting in the response of a tree to water stress. Our model illustrates how petiole flexibility can protect a water-stressed tree against the risk of cavitation. The mechanism, as described by our model, works as follows. Under water stress, turgor pressure and petiole rigidity decrease, making the leaves wilt. The increased leaf inclination reduces the direct solar irradiation and thus the leaf temperature. Consequently, transpiration decreases and so does the flow rate in the xylem. The reduced flow rate reduces the head loss, and thus the minimal pressure attained in the xylem will be less pronounced, reducing the risk of cavitation. This protective mechanism can be regarded as a passive form of paraheliotropism, as observed for example in arid land plants whose leaves reorient with the sun to protect themselves from excessive solar irradiation (Ehleringer and Forseth, 1980). Our model predicts that petiole flexibility can increase the minimal negative pressure reached in the xylem by about 0.5 MPa, which is a significant protection as compared to the typical pressure at which the onset of cavitation occurs, on the order of -1 to -2 MPa, depending on the species (Bond and Kavanagh, 1999; Sparks and Black, 1999; Koch et al., 2004).

Petiole flexibility also affects photosynthetic assimilation rates through leaf inclination, in a manner that depends on an interplay between tree geometry, petiole material properties, and water stress. Moderate petiole flexibility that deflects the average leaf inclination from upward-pointing to horizontal increases photosynthetic assimilation, whereas large flexibility that wilts the leaves downwards reduces photosynthetic assimilation. Remarkably, our model suggests that a flexible, nearly horizontal leaf may yield a larger photosynthetic assimilation rate than a rigid, horizontal leaf. Turgidity-dependent flexibility can smooth peak leaf temperatures at midday by slight wilting, thus preventing the reduction of electron transport at high temperatures that occurs in C_3 plants (Farquhar et al., 1980). Moreover, such transient wilting at midday, a phenomenon observed in nature (Chiariello et al., 1987), can protect the leaf's photosynthetic apparatus from permanent damage by overheating (Zhang et al., 2010).

We note that the described role of petiole flexibility in protecting the plant from water stress is not mutually exclusive with the existence of other water stress protection mechanisms, such as stomatal regulation or active control of osmotic pressure. Could we envision that the dominant protection afforded by petiole bending

arises through a different mechanism than reducing solar irradiation to the leaves? One alternative would be that petiole bending reduced hydrodynamic conductance, thus attenuating the minimal pressure under drought. The importance of this mechanism could be evaluated experimentally, by studying flow through an isolated petiole subjected to an imposed deflection. A similar experiment has recently been conducted by Lopez et al. (2014), who measured the flux through a segment of tree branch under deflection. They concluded that mechanical strain does not affect hydraulic conductivity.

In this paper we have studied the two paradigmatic cases of an isohydric tree (which decreases stomatal opening under water stress) and an idealized anisohydric tree (where stomatal opening is largely insensitive to water stress). We have shown that, for moderate water stress, petiole flexibility in an anisohydric tree can provide comparable protection against the risk of cavitation as stomatal closure does in an isohydric tree. Moreover, anisohydricity yields a larger photosynthetic assimilation rate than isohydricity. Both for isohydric and anisohydric trees, our model indicates that turgidity-dependent petiole flexibility significantly increases water use efficiency under water stress. These model predictions could be experimentally tested by using a setup similar to that of Chiariello et al. (1987), where tree leaves are supported by wires, thus preventing inclination changes. By measuring upper xylem pressure (Balling and Zimmermann, 1990; Wei et al., 2001) in free versus supported leaf configurations, one could establish the role of petiole flexibility in limiting the minimal pressure in a water-stressed tree.

Whereas this paper specifically focused on trees, the concepts presented here are extensible to other plants by accounting not only for petiole flexibility but also for stem flexibility. We emphasize that the central results presented in this paper, which indicate an important role of turgidity-dependent flexibility in protecting the plant against water stress, appear robust. Indeed, our conclusions, first deduced for a uniformly oriented foliage model, remained valid when considering distributed foliage angles, indicating that the effect of the flexibility-based protection mechanism does not vanish out when averaging among different leaf inclinations. Similarly, we expect our results to qualitatively remain valid if some of the simplifying hypotheses are relaxed. Thus, our model can be generalized to three-dimensional geometries by considering a 3D leaf orientation angle distribution. In 3D, the wilting movement will not necessarily be coplanar with the sun trajectory but, as in 2D, 3D wilting will protect the leaf from excessive solar irradiation. The current model neglects self-shading, and it is thus directly relevant to monolayer trees, but it can be generalized to account for self-shading in multilayer trees by modeling light–canopy interactions (see for instance Chelle and Andrieu, 2007). The anticipated robustness of our central results relies on the universality of the underlying mechanism: regardless of geometrical complexity and of the existence of additional processes not included in our model, in most plants a reduction of turgor pressure will increase leaf inclination angles, thus reducing leaf exposition to the sun and protecting the plant.

Acknowledgments

The authors thank the members of the Institut de Modélisation des Systèmes Vivants (IMSV) of University Paris-Saclay, and specially Andrée Tuzet, for valuable suggestions and discussions. We thank Loïc Tadrist for insightful discussions during the development of the model and Miguel Piñeirua as well as two anonymous reviewers for their careful reading of the manuscript and their suggestions to improve it. The first author was funded through the Grant ANR-11-IDEX-0003-02 of the IMSV project, in the framework of the IDEX “Paris-Saclay”.

Appendix A. Equations of the photosynthesis model

This appendix summarizes the equations of the photosynthesis model of Farquhar et al. (1980), as they are presented by Tuzet et al. (2003). The goal is to calculate the rate of CO_2 assimilation, given by

$$A = \min(V_c, V_j) - R_d, \tag{A.1}$$

where V_c and V_j are the assimilation rates limited by Rubisco and by RuBP respectively. In our calculation we neglect R_d, the rate of CO_2 evolution from processes other than photorespiration.

V_c is obtained from

$$V_c = V_{l,max}\frac{c_i - \Gamma_*}{c_i + K_c(1+o_i/K_o)}, \tag{A.2}$$

where $o_i = 0.210$ mol/mol and

$$V_{l,max} = \frac{V_{l,max}^{ref}\exp\{(E_{aV}/RT_{ref})(1-T_{ref}/T_l)\}}{1+\exp\{(ST_l - E_{dV})/RT_l\}}, \tag{A.3}$$

with $V_{l,max}^{ref} = 10^{-4}$ mol/(m^2 s), $E_{aV} = 58\,520$ J/mol, $E_{dV} = 220\,000$ J/mol, $S = 700$ J/(mol K), $T_{ref} = 293.2$ K, $R = 8.31$ J/(mol K), and T_l being the leaf temperature. K_c and K_o are computed from the following expression, where x stands for either c or o:

$$K_x = K_{x,ref}\exp\left\{\frac{E_x}{RT_{ref}}\left(1-\frac{T_{ref}}{T_l}\right)\right\}, \tag{A.4}$$

with $K_{o,ref} = 0.256$ mol/mol, $K_{c,ref} = 3.02\times10^{-4}$ mol/mol, $E_o = 36\,000$ J/mol, and $E_c = 59\,430$ J/mol. Γ_*, the CO_2 compensation point in the absence of day respiration, is obtained from

$$\Gamma_* = \gamma_0\left[1+\gamma_1(T_l - T_{ref}) + \gamma_2(T_l - T_{ref})^2\right], \tag{A.5}$$

with $\gamma_0 = 2.8\times10^{-5}$ mol/mol, $\gamma_1 = 5.09\times10^{-2}$ K^{-1}, and $\gamma_2 = 1.0\times10^{-3}$ K^{-2}.

V_j is obtained from

$$V_j = \frac{J}{4}\frac{(c_i - \Gamma_*)}{(c_i + 2\Gamma_*)}, \tag{A.6}$$

where J is obtained from

$$\Theta J^2 - (\alpha Q_{phot} + J_{l,max})J + \alpha Q_{phot} J_{l,max} = 0, \tag{A.7}$$

where $\alpha = 0.2$ and $\Theta = 0.9$ Q_{phot} is the absorbed photon irradiance, which we assume proportional to the visible radiation received by the leaf:

$$Q_{phot} = \lambda_Q a_V S_0 \cos(\phi_S)\{\sin[\min(\max(\mathrm{sign}(\phi)(\phi - \phi_S), 0), \pi)] + r\}, \tag{A.8}$$

where $\lambda_Q \approx 4.6\times10^{-6}$ mol/J is the fraction of visible radiation useful for photosynthesis.

The remaining unknown in the above equations is c_i, the CO_2 concentration in the stomatal cavity. To compute c_i, we impose

$$A = g_{CO2}(c_v - c_i), \tag{A.9}$$

where $g_{CO2} = g_s/1.6$ and $c_v \approx 4\times10^{-4}$ mol/mol is the atmospheric CO_2 concentration. It is noted that Eq. (A.9) neglects the boundary layer resistance to CO_2 diffusion, which is assumed limited by stomatal conductance. Eqs. (A.1) and (A.9) constitute a system of two equations, from which the values of the two unknowns, c_i and A, can be obtained.

References

Allen, C.D., Macalady, A.K., Chenchouni, H., Bachelet, D., McDowell, N., Vennetier, M., Kitzberger, R., Rigling, A., Breshears, D.D., Hogg, E.H., Gonzalez, P., Fensham, R., Zhang, Z., Castro, J., Demidova, N., Lim, J.-H., Allard, G., Running, S.W., Semerci, A., Cobb, N., 2010. A global overview of drought and heat-induced tree mortality reveals emerging climate change risks for forests. For. Ecol. Manag. 259, 660–684.

Balling, A., Zimmermann, U., 1990. Comparative measurements of the xylem pressure of Nicotiana plants by means of the pressure bomb and pressure probe. Planta 182, 325–338.

Bond, B.J., Kavanagh, K.L., 1999. Stomatal behavior of four woody species in relation to leaf-specific hydraulic conductance and threshold water potential. Tree Physiol. 19, 503–510.

Buckley, T., 2005. The control of stomata by water balance. New Phytol. 168, 275–292.

Chelle, M., Andrieu, B., 2007. Functional–Structural Plant Modelling in Crop Production Modeling Light Environment of Virtual Plants. Springer, Amsterdam, Netherlands, pp. 75–89 (Chapter 7).

Chiariello, N.R., Field, C.B., Mooney, H.A., 1987. Midday wilting in a tropical pioneer tree. Funct. Ecol. 1, 3–11.

Cochard, H., 2006. Cavitation in trees. C. R. Phys. 7, 1018–1026.

Ehleringer, J., Forseth, I., 1980. Solar tracking by plants. Science 210, 1094–1098.

Engelbrecht, B.M.J., Tyree, M.T., Kursar, T.A., 2007. Visual assessment of wilting as a measure of leaf water potential and seedling drought survival. J. Trop. Ecol. 23, 497–500.

Farquhar, G.D., von Caemmerer, S., Berry, J.A., 1980. A biochemical model of photosynthetic CO2 assimilation in leaves of C3 species. Planta 149, 78–90.

Incropera, F.P., De Witt, D.P., 1985. Fundamentals of Heat and Mass Transfer, 2nd edition. John Wiley & Sons, Hoboken, New Jersey, USA.

Koch, G.W., Sillett, S.C., Jennings, G.M., Davis, S.D., 2004. The limits to tree height. Nature 428, 851–854.

Leigh, A., Sevanto, S., Ball, M.C., Close, J.D., Ellsworth, D.S., Knight, C.A., Nicotra, A.B., Vogel, S., 2012. Do thick leaves avoid thermal damage in critically low wind speeds? New Phytol. 194, 477–487.

Lopez, R., Badel, E., Peraudeau, S., Leblanc-Fournier, N., Beaujard, F., Julien, J.-L., Cochard, H., Moulia, B., 2014. Tree shoot bending generates hydraulic pressure pulses: a new long-distance signal?. J. Exp. Bot. 65, 1997–2008.

McDowell, N., Pockman, W.T., Allen, C.D., Breshears, D.D., Cobb, N., Kolb, T., Plaut, J., Sperry, J., West, A., Williams, D.G., Yepez, E.A., 2008. Mechanisms of plant survival and mortality during drought: why do some plants survive while others succumb to drought?. New Phytol. 178, 719–739.

Murphy, R., Ortega, J.K.E., 1996. A study of the stationary volumetric elastic modulus during dehydration and rehydration of stems of pea seedlings. Plant Physiol. 110, 1309–1316.

Niklas, K.J., Spatz, H.-C., 2012. Plant Physics. The University of Chicago Press, Chicago, Illinois, United States.

Nilsson, S.B., Hertz, C.H., Falk, S., 1958. On the relation between turgor pressure and tissue rigidity. II Theoretical calculations on model systems. Physiol. Plant. 11, 818–837.

Nobel, P.S., 2005. Physicochemical and Environmental Plant Physiology. Elsevier Academic Press, Amsterdam, Netherlands.

Sade, N., Gebremedhin, A., Moshelion, M., 2012. Risk-taking plants: anisohydric behavior as a stress-resistance trait. Plant Signal Behav. 7, 767–770.

Saltelli, A., Tarantola, S., Campolongo, F., Ratto, M., 2004. Sensitivity Analysis in Practice. Wiley, Hoboken, New Jersey, United States.

Sparks, J.P., Black, A., 1999. Regulation of water loss in populations of *Populus trichocarpa*: the role of stomatal control in preventing xylem cavitation. Tree Physiol. 19, 453–459.

Tadrist, L., Saudreau, M., de Langre, E., 2014. Wind and gravity mechanical effects on leaf inclination angles. J. Theor. Biol. 341, 9–16.

Tuzet, A., Perrier, A., 2008. Modeling the dynamics of water flow through plants, role of capacitance in stomatal conductance, and plant water relations. In: Response of Crops to Limited Water: Understanding and Modeling Water Stress Effects on Plant Growth Processes. American Society of Agronomy, Madison, Wisconsin, United States, pp. 145–164 (Chapter 5).

Tuzet, A., Perrier, A., Leuning, R., 2003. A coupled model of stomatal conductance, photosynthesis and transpiration. Plant Cell Environ. 26, 1097–1116.

Wei, C., Steudle, E., Tyree, M.T., Lintilhac, P.M., 2001. The essentials of direct xylem pressure measurement. Plant Cell Environ. 24, 549–555.

Wu, Q.-L., Cournède, P.-H., Mathieu, A., 2012. An efficient computational method for global sensitivity analysis and its application to tree growth modelling. Reliab. Eng. Syst. Saf. 107, 35–43.

Zhang, Y.-L., Zhang, H.-Z., Du, M.-W., Li, W., Luo, H.-H., Chow, W.-S., Zhang, W.-F., 2010. Leaf wilting movement can protect water-stressed cotton (*Gossypium hirsutum* L.) plants against photoinhibition of photosynthesis and maintain carbon assimilation in the field. J. Plant Biol. 53, 52–60.